

An Atom Laser is not monochromatic

S. Choi¹, D. Strömberg^{1,2}, and B. Sundaram¹

¹. *Department of Physics, University of Massachusetts, Boston, MA 02125, USA*

². *Department of Information Technology, Uppsala University, 751 05 Uppsala, Sweden*

We study both numerically and analytically the possibility of using an adiabatic passage control method to construct a Mach-Zehnder interferometer (MZI) for Bose-Einstein condensates (BECs) in the time domain, in exact one-to-one correspondence with the traditional optical MZI that involves two beam splitters and two mirrors. The interference fringes one obtains from such a minimum-disturbance set up clearly demonstrates that, fundamentally, an atom laser is not monochromatic due to interatomic interactions. We also consider how the amount of entanglement in the system correlates to the interference fringes.

PACS numbers: 03.75.Dg, 03.75.Kk, 03.75.Lm

Atomic Bose-Einstein condensates (BECs) are often referred to as the “atom laser,” the matter-wave equivalent of a laser. Unlike massless photons from a laser which do not interact, atoms from an atom laser do interact with each other, and so far it has not been clearly established how and to what extent the monochromaticity of an atom laser is compromised by such interactions. The term “atom laser” is not yet defined universally other than in a broad general sense, although there have been attempts to be more specific about what an atom laser should be, including the directionality of the beam in a close analogy with a laser [1]. However, given fundamental differences such as the fact that the atoms in a BEC are intrinsically stationary, here we shall use the term to denote an *intense* source of *coherent* atoms *for atom optical transformations* such as reflection, refraction and beam splitting.

In general, the non-zero mass of the atoms necessitates rather elaborate and experimentally demanding schemes to coherently accelerate and guide the matter-wave. In order to mitigate this problem, we propose the use of atom optics in the *time-domain* based on adiabatic passage. An important reason for this is that time domain atom optics is less prone to decoherence due to, say, atom losses as compared to techniques such as guiding a BEC in space. Further, the adiabatic passage method is a well-known technique in quantum mechanics that provides a way to “delicately” control a quantum system via slow passage along the energy landscape, while preserving the quantum system in one of the energy eigenstates, typically the ground state. By minimizing any disturbance, and maintaining the condensate in the ground state, one can draw conclusions about the intrinsic properties of an atom laser unmodified by such additional actions as ballistic expansion.

To address the question of the monochromaticity of an atom laser, we model both numerically and analytically an ideal Mach-Zehnder Interferometer (MZI) for BECs in the time domain and deduce the spectral composition of an atom laser from the interference pattern generated. The construction of a MZI that uses BEC as the source of coherent atoms is one of the goals in atom optics owing to the promise of, for instance, high precision matter-wave

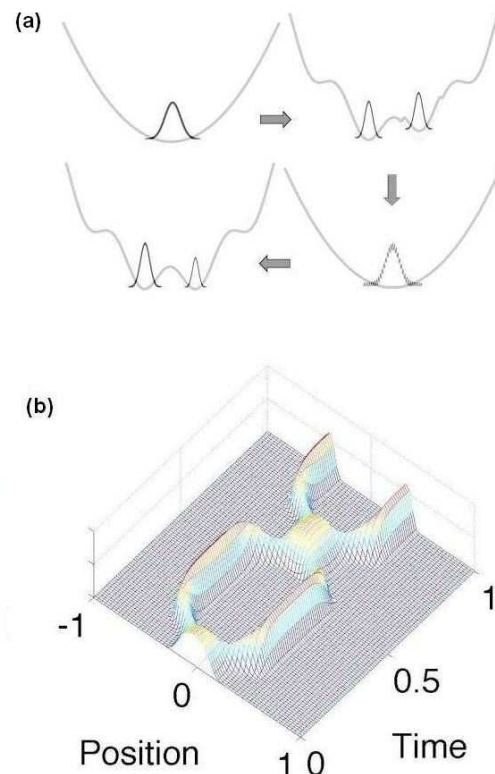


FIG. 1: (a) Schematic diagram of the transformations that the potential undergoes over time, starting with beam splitting, addition of a potential step, recombination and final beam splitting. (b) Spatio-temporal probability density obtained by solving the Gross-Pitaevkii equation describing the condensate passing through the time-domain MZI.

based metrology. In a typical optical MZI scheme, coherent light from a laser is passed through a beam splitter which sends the light beam into two paths; one of the beams passes through a phase shifter and the two beams are then recombined by reflecting off mirrors onto a second beam splitter. The phase shift experienced in one arm is reflected in the intensity variation at the two detectors. We have simulated the time-domain MZI by adding an optical potential to the usual quadratic trapping potential and adiabatically varying its amplitude to

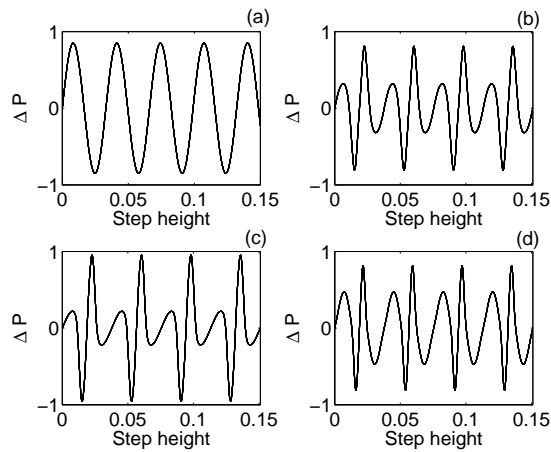


FIG. 2: Interference fringes obtained by solving the Gross-Pitaevskii Equation (GPE) to model the time-domain MZI for various values of the nonlinearity constant g (a) $g = 0$ (b) $g = 0.5$ (c) $g = 5$ (d) $g = 10$. The sinusoidal fringe for the linear $g = 0$ case is clearly modified for $g > 0$ i.e. in the presence of interatomic interactions, showing that the atom laser is no longer monochromatic.

simulate exactly the action of the optical elements in an usual MZI, namely the two beam splitters, mirrors and wave guides. The phase shift is provided by adding an additional potential step to one “arm” of the interferometer. Given the adiabatic nature of the method, the two arms do not interfere unless they are explicitly recombined by way of the second beam splitter. The population difference ΔP between the two arms is finally measured as a function of the step height. A schematic diagram of the required operations is provided in Fig. 1(a). To the best of our knowledge, such a scheme has not yet been experimentally implemented, although there have been several experiments on interference of BEC in optical potentials [2] and in atom chips [3, 4, 5], with the important difference that all of these release the condensates to expand ballistically after the first beam splitter. The time-domain MZI proposed here keeps the condensate in the ground state, better revealing the nature of the atom laser.

The Gross-Pitaevskii Equation (GPE) was used to simulate the dynamics of the condensate in the presence of the spatio-temporal potential. The GPE has been extremely successful in describing the dynamics of BECs under a variety of experimental conditions including optical lattices[6]. Specifically, we consider the 1-D GPE:

$$i\hbar \frac{\partial \psi}{\partial t} = \left[-\frac{\hbar^2}{2m} \frac{d^2}{dx^2} + V(x, t) + g|\psi(x, t)|^2 \right] \psi(x, t) \quad (1)$$

where $\psi(x, t)$ denotes the condensate mean field and $V(x, t)$ denotes the adiabatically changing time-dependent potential. As shown later in our analysis, the dimensionality of the GPE simulation does not affect the final results. We always retain the parabolic trapping potential, so $V(x, t) = \frac{1}{2}m\omega_t x^2 + Af(t) \cos(kx) +$

$V_{step}(x, T_{1/4} < t < 2T_{1/4})$ where $k = 2\pi/\lambda$, A is the amplitude of the optical lattice potential and $T_{1/4}$ denotes 1/4 of the total duration of the simulation T . $f(t)$ provides the time dependence for the adiabatically changing amplitude of the optical lattice:

$$f(t) = \begin{cases} t/T_{1/4} & 0 < t < T_{1/4}, \text{ first beam splitter;} \\ 1 & T_{1/4} < t < 2T_{1/4}, \text{ first beam splitter;} \\ (3 - t/T_{1/4}) & 2T_{1/4} < t < 3T_{1/4}, \text{ recombination;} \\ (t/T_{1/4} - 3) & 3T_{1/4} < t < 4T_{1/4}, \text{ final beam splitter.} \end{cases} \quad (2)$$

The potential step was introduced during $T_{1/4} < t < 2T_{1/4}$ using a super-Gaussian in one arm $V_{step}(x, t) = \hbar e^{-[(t-T_{1/4})/\sigma_t]^{10}} e^{-[(x-\lambda/2)/\sigma_x]^{30}}$, with the spatial and temporal width of $\sigma_x = \lambda/3$ and $\sigma_t = T_{1/4}/2$ respectively. The probability density of the condensate obtained from GPE dynamics with $g = 5$, $A = 25$, $T_{1/4} = 400$, and $\lambda = 15$ in harmonic oscillator units of the initial trapping potential is shown in Fig. 1(b) as a spatio-temporal plot. As is clear from the figure, the simulation provides exact one-to-one correspondence to the MZI, and the adiabatic condition ensures that the wave function evolves extremely cleanly. One of the advantages of this scheme of interferometry is that the area enclosed by the two arms of the interferometer is readily controllable by changing λ ; in particular, with a larger enclosed area, higher sensitivity is possible for use in, for instance, interferometric rotational sensors used in space navigation.

We plot in Fig. 2 the final intensity difference as a function of step height h for different values of nonlinearity g . It is noted that a relatively large phase shift is recorded even for small variations in step height, indicating high sensitivity of the condensate to changes in potential height. In the linear case (non BEC) $g = 0$ one obtains perfect sinusoidal variation as a function of h , while for $g > 0$, the pattern clearly deviates from the sinusoidal, implying that an atom laser loses monochromaticity due to the presence of interatomic interactions. This is confirmed by a Fourier transform which reveals four closely spaced frequency components.

In order to better understand this result and to ensure that the adiabatic assumptions are not violated, a detailed analysis of this system can be given as follows. First, we assume that the adiabatic passage we used above preserves the single mode approximation. The condensate after beam splitting and the potential step (which imparts relative phase of Θ) may then be written as:

$$\hat{\psi}(x, t, \Theta) = \phi_L(x, d)\hat{a}_L(t) + \phi_R(x, d) \exp(i\Theta)\hat{a}_R(t) \quad (3)$$

where $\hat{a}_{L(R)}(t)$ are bosonic annihilation operators for the modes of the matter wave field in the left and right arms and $\phi_{L(R)}(x, d)$ are the corresponding spatial mode functions. These may be approximated by spatial functions such as shifted Gaussians $\phi_{L(R)}(x, d) = (\pi\sigma^2)^{-1/4} e^{-(x\pm d)^2/4\sigma^2}$ that, under adiabatic evolution, do not change shape. The phase shift has been modeled by the explicit insertion of the $\exp(i\Theta)$ term, which

is clearly an approximation to the full GPE simulation where the phase shift results from the passage of the condensate over a potential step in one arm. The analysis is therefore best suited to the cases with lower values of g for which interplay between the potential step and repulsive atomic interactions do not complicate the phase relationship given in Eq. (3).

Since we use the adiabatic passage method, there are no additional net physical effects on the BEC undergoing the remaining two operations that constitute the MZI (recombination and then second beam splitting), other than those of the interatomic scattering and the natural tunnelling flow between the left and right arms. This is due to the Josephson effect and the geometry of the system though the tunnelling would be minimized when the arms are well separated. The effective interference fringes are then given by the difference in the number of atoms in the two arms after the system has evolved a certain time τ through the MZI. With the field decomposition of Eq. (3) the bosonic Hamiltonian is given by

$$\hat{H} = \hbar\omega(\hat{a}_L^\dagger\hat{a}_L + \hat{a}_R^\dagger\hat{a}_R) + \frac{\Delta E(t)}{2}[\hat{a}_L^\dagger\hat{a}_R + \hat{a}_R^\dagger\hat{a}_L] + g(\hat{a}_L^{\dagger 2}\hat{a}_L^2 + \hat{a}_R^{\dagger 2}\hat{a}_R^2) \quad (4)$$

where $\Delta E(t) = \hbar\omega \exp[-d^2(t)/\sigma^2]$ gives the overlap of the two spatial modes and is the time-dependent tunneling energy. This overlap clearly depends on the dimensionality of the modes. However, change in dimensionality merely alters this single scaling parameter and not the behavior we describe. This Hamiltonian is also well-known as the Hamiltonian that describes two-component BECs when ‘‘L’’ and ‘‘R’’ denote two different species instead of the left and right arms. Introducing the Schwinger angular momentum operators, $\hat{J}_{+(-)} = \hat{a}_{L(R)}^\dagger\hat{a}_{R(L)}$ and $\hat{J}_z = \frac{1}{2}(\hat{a}_L^\dagger\hat{a}_L - \hat{a}_R^\dagger\hat{a}_R)$, the Hamiltonian is equivalent to a ‘‘Lipkin-Meshkov-Glick’’ type Hamiltonian [7],

$$\hat{H} = \frac{\Delta E(t)}{2}(\hat{J}_+e^{i\Theta} + \hat{J}_-e^{-i\Theta}) + 2g\hat{J}_z^2. \quad (5)$$

The time evolution operator corresponding to this nonlinear Hamiltonian has been studied previously [8]. The measured intensity difference is given by $\langle J_z(\tau) \rangle$ at time τ , $\langle \hat{J}_z(\tau, \Theta) \rangle = \langle \hat{R}^\dagger e^{iH'\tau} \hat{R} \hat{J}_z \hat{R}^\dagger e^{-iH'\tau} \hat{R} \rangle$, where $\hat{R} = \exp\left[-\frac{\pi}{4}(\hat{J}_-e^{-i\Theta} - \hat{J}_+e^{i\Theta})\right]$ is the well-known rotation operator and H' is the transformed Hamiltonian diagonal in \hat{J}_z : $\hat{H}' = \hat{R}\hat{H}\hat{R}^\dagger - i\hat{R}\frac{\partial}{\partial t}\hat{R}^\dagger \equiv \Delta E\hat{J}_z - g\hat{J}_z^2$.

Writing the quantum state in a general form $|\Psi\rangle = \sum_m c_m |m\rangle_L |N-m\rangle_R$ where N is the total number of atoms in the system, one obtains,

$$\begin{aligned} \langle \hat{J}_z(\tau, \Theta) \rangle &= -\frac{e^{ig\tau}}{2} \left(\sum_{m'} \beta_{m'}^{(+)} \gamma_{m'}^{(+)*} \right) e^{i(\Theta + \Delta\omega\tau)} \\ &\quad - \frac{e^{ig\tau}}{2} \left(\sum_{m'} \beta_{m'}^{(-)} \gamma_{m'}^{(-)*} \right) e^{-i(\Theta + \Delta\omega\tau)} \end{aligned}$$

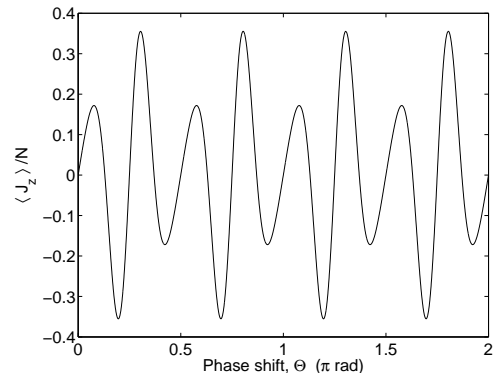


FIG. 3: The interference fringe given by the fractional number difference in the two arms of the interferometer, $\langle \hat{J}_z \rangle / N$, obtained using the analytical methods under the adiabatic assumption. The figure, which shows remarkable agreement with the simulation results obtained above using the GPE, again clearly indicates the presence of several frequency components in the atom laser from the way it deviates from the sinusoidal pattern.

where $\Delta\omega = \Delta E/\hbar$ and

$$\begin{aligned} \beta_{m'}^{(\pm)} &\equiv \sum_m c_m^* \mathcal{R}_{m,m'} \sqrt{j(j+1) - m'(m' \pm 1)} \\ \gamma_{m'}^{(\pm)} &\equiv \sum_m c_m^* \mathcal{R}_{m,m' \pm 1} e^{\pm i 2m' g\tau} \end{aligned} \quad (6)$$

with the matrix elements $\mathcal{R}_{m,m'} \equiv \langle m | \hat{R}^\dagger | m' \rangle$ provided by an analytical expression [9].

A natural choice of quantum state for the two component BECs with a relative phase Θ is a coherent spin state or the Bloch state with equal number of atoms in both arms such that $|\Psi\rangle = |\theta = \pi/2, \phi = \Theta\rangle$. In this case, the coefficients $c_m = (C_{j+m}^{2j})^{1/2} e^{i(j-m)\Theta} / 2^j$ where C_m^n denotes the combination, $C_m^n = n! / [(n-m)!m!]$. The resulting interference fringe with $(\Delta\omega)\tau$ chosen to be $(2n+2)\pi$ and $g\tau = (2n + \frac{3}{2})\pi$, where n is an integer, is plotted in Fig. 3 which shows remarkable agreement with the result from the GPE simulation. With $n \approx 127$, we are simulating the $g = 0.5$ case in the GPE simulation above, and the effective magnitude of g of the order $\frac{3}{2N}$ places the system in the Josephson regime. The amplitudes are different from the GPE simulation simply due to our choice of $\langle \hat{J}_z \rangle$ to be half the atom number difference.

The results confirm that the coherent spin state is a natural state for BECs with relative phase arising from the adiabatic passage method. With the current system, the initial state prepared at the first beam splitter can be controlled so that the number of atoms in each arm are not equally distributed. For instance, this can be accomplished by adiabatically deforming the potential wells asymmetrically to collect more atoms in one arm and then continue adiabatically to model subsequent actions such as recombination. In such cases, a coherent spin state with $\theta \neq \pi/2$ can be generated, and consequently

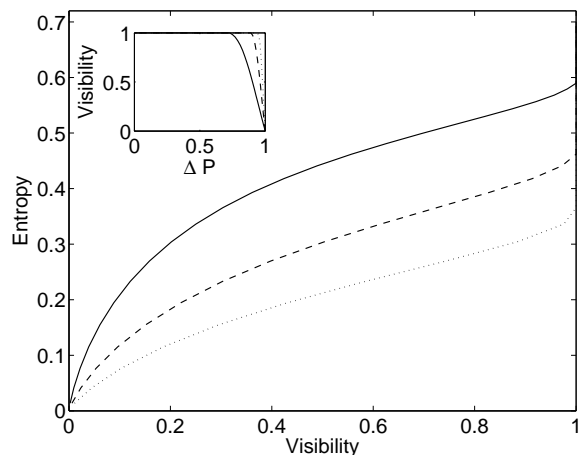


FIG. 4: Entanglement parameterized by the von Neumann entropy of the input state plotted against the visibility of the final inference fringes. Inset: Visibility vs. fractional atom number difference between the two arms ΔP of the input state. Solid, dashed, and dotted lines: equivalent nonlinearity in GPE of $g = 0, 0.25$ and 0.5 respectively in both the main figure and the inset.

the amount of entanglement between the left and right arms is directly controllable. The state with $\theta = \pi/2$ has the largest entanglement while the state with $\theta = 0$ has the least amount of entanglement [8].

Finally, how the presence of interatomic interaction modifies the connection between the fringe visibility and entanglement is of interest from the point of possible experimental determination of parameters such as the interatomic scattering length using this method. The degree of entanglement between the left and right arms can be quantified using the von Neumann entropy $E(t) = -\frac{1}{\log_2(N+1)} \sum_{m=-j}^j |c_m|^2 \log_2 |c_m|^2$, which is clearly connected to the interference pattern at time τ given by $\langle \hat{J}_z(\tau, \Theta) \rangle$. We plot in Fig. 4 the von Neumann entropy of the input state against visibility \mathcal{V} of the fringes $\mathcal{V} = (I_{max} - I_{min}) / (I_{max} + I_{min})$ where $I = |\langle \hat{J}_z(\tau) \rangle|^2$ denotes the intensity of the fringe pattern. The visibility of the interference fringes is obviously reduced with an asymmetric beam splitting that corresponds to $\theta \neq \pi/2$.

The different line shapes correspond to different values of nonlinearity. For a given value of visibility one obtains lower entanglement with higher nonlinearity. This initially counterintuitive result can be understood from the inset of Fig. 4, which provides the relationship between the fractional number difference between the two arms of the initial input state ΔP and the visibility of the fringes. As expected $\mathcal{V} \rightarrow 0$ as $\Delta P \rightarrow 1$. For $\Delta P < 0.75$, \mathcal{V} already reaches 1 as one starts finding atoms in the other arm such that $\langle \hat{J}_z \rangle$ starts to take on negative values as a function of Θ . With higher nonlinearity one finds $\mathcal{V} \rightarrow 1$ even for larger values of ΔP . This may be understood as the result of higher entanglement due to collisions. With higher entanglement, the “wave-like” nature of the wave function is enhanced (changing one arm affects the other arm instantaneously) which encourages tunneling between the two arms, and subsequently higher visibility.

In conclusion, we have studied a potentially realizable scheme for a MZI using BECs. The resulting intensity difference between the two arms as a function of phase shift is found to demonstrate that, fundamentally, an atom laser is not monochromatic but rather comprises of a number of frequency components. The adiabatic passage method ensured that the only “alteration” made to the condensate is that of coherent splitting and the establishment of a relative phase between the two arms which naturally puts the trapped condensate onto a coherent spin state. The dynamics of the split condensate was then given simply by a standard many-body Hamiltonian over a finite time interval. The fact that monochromaticity is lost even in this idealized model implies that one should exercise caution when discussing an atom laser as simply a matter-wave equivalent of a laser, since additional effects such as decoherence due to atom losses is expected to degrade the quality even further. Finally we observed that with higher nonlinearity, higher fringe visibility can be obtained with very uneven beam splitting owing to the enhanced entanglement between the two arms. This work suggests that there are many new aspects to be explored in the time domain quantum control of BEC using adiabatic passage.

-
- [1] H. M. Wiseman, Phys. Rev. A **56**, 2068 (1997)
[2] Y. Shin, M. Saba, T. A. Pasquini, W. Ketterle, D.E. Pritchard, and A.E. Leanhardt, Phys. Rev. Lett. **92**, 050405 (2004)
[3] Y. Shin, C. Sanner, G.-B. Jo, T. A. Pasquini, M. Saba, W. Ketterle, D. E. Pritchard, M. Vengalattore and M. Prentiss, Phys. Rev. A **72**, 021604(R) (2005)
[4] G.-B. Jo, Y. Shin, S. Will, T. A. Pasquini, M. Saba, W. Ketterle, D. E. Pritchard, M. Vengalattore, and M. Prentiss, Phys. Rev. Lett. **98**, 030407 (2007)
[5] G.-B. Jo, J.-H. Choi, C. A. Christensen, T. A. Pasquini, Y.-R. Lee, W. Ketterle, and D. E. Pritchard, Phys. Rev. Lett. **98**, 180401 (2007)
[6] O. Morsch and M. Oberthaler, Rev. Mod. Phys. **78**, 179 (2006)
[7] H. J. Lipkin, N. Meshkov, and N. Glick, Nucl. Phys. A **62** 188 (1965)
[8] S. Choi, and N. P. Bigelow, Phys. Rev. A **72** 033612 (2005)
[9] F. T. Arrechi, E. Courtens, R. Gilmore, and H. Thomas, Phys. Rev. A **6**, 2211 (1972)